Journal of Structural Geology, Vol. 11, No. 5, pp. 553 to 568, 1989

The Caledonian Skerrols Thrust, SW Scotland—microstructure and strain

DILIP SAHA

Geological Studies Unit, Indian Statistical Institute, 203 Barrackpore Trunk Road, Calcutta—700 035, India

(*Received* 24 *November* 1986; *accepted in revised form* 25 *January* 1989)

Abstract—Strain measurements from quartz grain shapes in deformed Jura Quartzite around Loch Skerrols, Islay, SW Scotland, indicate that a strain gradient is associated with the Loch Skerrols Thrust which separates the Jura Quartzite from the Bowmore Sandstone. Progressive strain is associated with microstructural changes in the form of grain refinement through to dynamic recrystallization. The maximum observed ratio of intracrystalline strain is 1.9:1.3:0.4, $\xi_a = 1.1$. The X-axis of the finite-strain ellipsoid is close to the mesoscopic lineation in quartz-mylonites in the thrust belt and the XY plane is sub-parallel to the foliation. The apparent flattening strain may be explained by superposition of simple shear (thrust regime) on initial flattening strain associated with the earlier stages of progressive development of the Islay Anticline. This implies that the Loch Skerrols Thrust is comparable to a break thrust. Strain-induced quartz c-axis preferred orientation increases in intensity as the thrust is approached. At a higher strain the fabric is a type-I cross-girdle pattern with a point maximum within 20° of Z. Fabric asymmetry, both internal and with respect to an external frame, defined by the principal strain directions, attests to a westward transport of Dalradian Jura Quartzite on the thrust.

INTRODUCTION

THE Loch Skerrols Thrust separates the Bowmore Sandstone from the Dalradian sequence of NE Islay (Fig. 1). It follows a sinuous southward course from Bun-an-Uillt on the eastern shore of Loch Gruinart and crosses Loch Skerrols. South of Loch Skerrols, the course of the thrust plane is less certain due to poor exposure in the area. Wilkinson *et al.* (1907) traced the thrust plane, offset by a normal fault, near Tallant Farm (Fig. 1a). Beyond this point its course is concealed under superficial deposits, but it probably continues to the shore of Laggan Bay (Wilkinson *et al.* 1907, Bailey 1917, Amos 1959, cf. Fitches & Maltman 1984).

The Loch Skerrols Thrust is thought to represent a major dislocation in Scotland. Although Kennedy (1946) and Garson & Plant (1972) differ in their reconstruction along the Great Glen Fault, all these authors suggested that the logical southerly continuation of the Moine Thrust is the Loch Skerrols Thrust in Islay. However, in contrast to the NW Highlands, Dalradian rather than the Moine rocks lie on top of the Loch Skerrols Thrust in Islay. On the other hand, Borradaile (1979) notes that "greater total strains have not been recorded from the vicinity of the Loch Skerrols Thrust". Fitches & Maltman (1984) consider the thrust just as one element in a major flat-lying NW-directed ductile shear zone and suggest that the Bowmore Sandstone (Group) is a lateral equivalent of the Crinan Grits in the Dalradian Supergroup, thus implying limited stratigraphical and structural discontinuity across the Loch Skerrols Thrust. More recently, the structure has been considered to be due to rejuvenation of an earlier basin margin fault bounding the Dalradian (Anderton 1988). Although most workers agree that there is considerable movement along the Loch Skerrols Thrust, no systematic study of strain and microstructures in the thrust zone has been made.

The best available exposure of the thrust zone is in the Loch Skerrols—An Carn area. Exposures of sheared Jura Quartzite are scattered in a narrow belt stretching from NE of Knockdon through An Carn to Loch Drolsay (see Fig. 1b). The junction between the Bowmore Sandstone and the Dalradian Jura Quartzite is also exposed on the eastern shore of Loch Gruinart near Bun-an-Uillt.

On a traverse across the thrust zone from Loch Cam in the east to Knockdon in the west, the available exposures were studied in detail to observe and measure thrust related minor structures; specimens were collected for three-dimensional strain measurement, microstructural and quartz c-axis fabric studies. The results of strain and fabric measurement are described here and their implications to the development of the Loch Skerrols Thrust and the Islay Anticline discussed.

MESOSCOPIC STRUCTURES IN THE THRUST ZONE

A traverse from Loch Cam to An Carn

A traverse westward from the west shore of Loch Cam to the summit of An Carn shows a gradual change in the lithology of the Jura Quartzite. Near Loch Cam and northwest of the loch, individual clastic grains can be recognized. These have a weak flattening shape fabric and their sub-parallel alignment defines a patchy foliation in the rock. Near Drolsay River, there is the first appearance of a streaky lineation on foliation in quartzite. Where the clastic grains are obvious they show an apparent elongation parallel to this lineation. Farther west on the southern slope of An Carn, the white quartzite breaks along a low-angle, SE-dipping foliation which locally wraps around augen of relatively undeformed quartzite. A lineation is defined by parallel

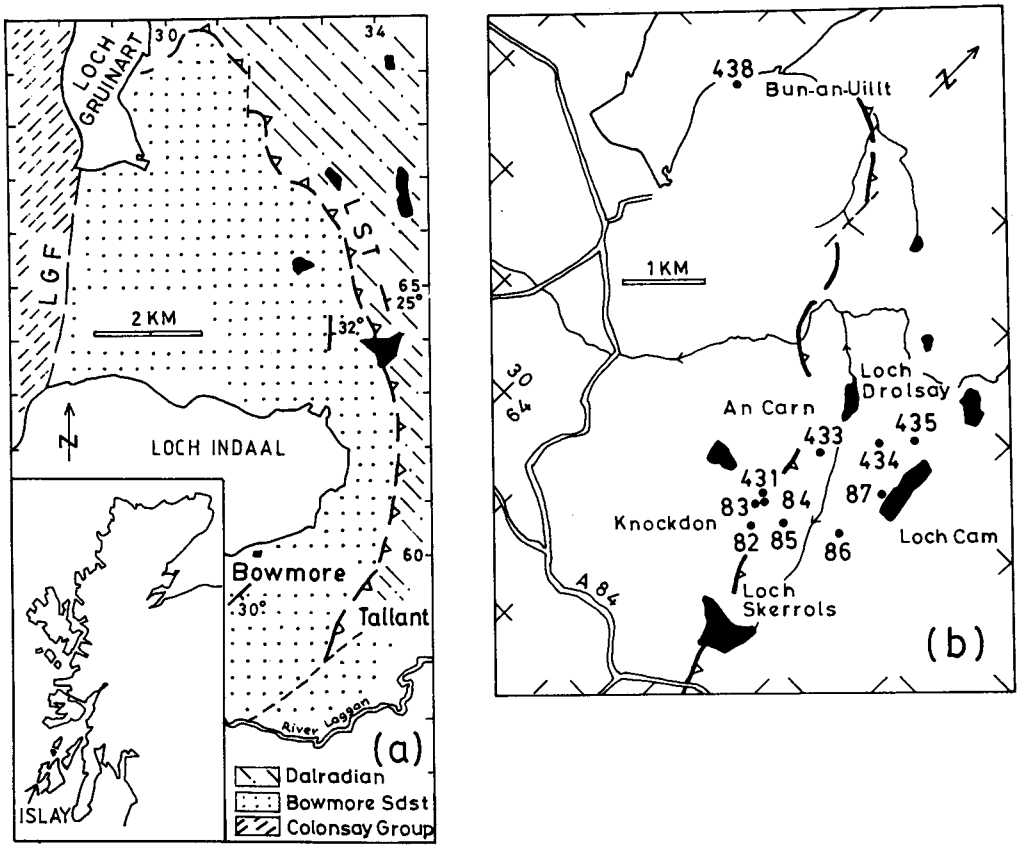

Fig. 1. (a) Geologic setting and location map, Loch Skerrols Thrust, Islay. The locations of specimens collected for strain and fabric studies are shown in (b). LST = Loch Skerrols Thrust, LGF = Loch Gruinant Fault.

alignment of mica flakes. Individual clastic grains are difficult to distinguish in hand specimen and the rock as a whole appears to be much finer grained. The foliation in the thrust zone dips 30–40° SSE and the lineation plunges at a low angle towards SSE, but is not exactly down-dip on foliation (Fig. 2).

Bun-an-Uillt area

The area described below includes the section of intermittent exposures that straddles the high-tide level along the eastern shore of Loch Gruinart between a point about 0.5 km southwest of Bun-an-Uillt Farm and Crois-Mhor. The rocks in the southern half of the section are shattered and often traversed by bands and veins of breccia or fault gouge, which is related to a fault independent of the Loch Skerrols structure.

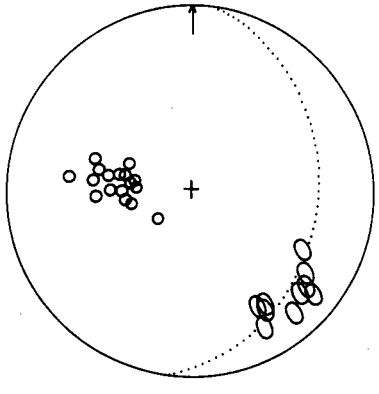

Fig. 2. Equal-area plot of foliation poles (circles) and mineral elongation lineations (ellipses) in Loch Skerrols thrust zone. The girdle gives the average orientation of foliation.

In a small exposure about 300 m southwest of the farmhouse [296693], intact blocks of a micaceous quartzite have the appearance of a platy mylonite. Although the foliation is undulatory due to the presence of open crenulations on axes plunging gently WSW, the overall dip is 20°S. A lineation defined by parallel grooves on polished foliation surfaces, and parallel alignment of white mica is persistent throughout the exposure, and has an E–W trend. The lineation is gently curved around hinges of later minor folds.

From the shore opposite Bun-an-Uillt farmhouse to Crois-Mhor buff coloured quartzite has a penetrative foliation dipping 60–70° WNW and defined by the alignment of flattened sand-sized grains. A lineation is also observed, which plunges roughly down-dip on foliation. This reversal in dip of the mylonitic foliation between An Carn and Bun-an-Uillt is probably related to folding of the Loch Skerrols Thrust. The E–W trend of foliation southwest of Bun-an-Uillt farmhouse can be explained as due to a drag effect along an E–W fault that has displaced the Loch Skerrols Thrust (Amos 1959). Moreover, minor crenulations and brittle shears are overprinted on the mylonitic foliation in this area.

STRAIN ANALYSIS

Method

Strain measurements relate to deformed Jura Quartzite in the vicinity of Loch Skerrols Thrust. For practical purposes the western boundary of the outcrop of the Jura Quartzite is taken as within a few metres of the thrust. Details of deformation microstructures are presented in a later section. In general, thin sections of deformed Jura Quartzite show relatively larger grains of quartz (*clast*) surrounded by finer (30–40 μm) grains of quartz (*matrix*). The clast sizes are at least an order of magnitude larger than the *matrix* grains. Two-dimensional strain was determined for each of three mutually perpendicular thin sections cut from hand specimens of Jura Quartzite collected at various localities in the thrust zone (Fig. 1b). In each thin section strain ratios were obtained from quartz clasts using the R_f/ϕ method (Ramsay 1967, Dunnet 1969); a few representative plots are shown in Fig. 3. The strain values thus obtained were cross-checked using an algebraic method of Robin (1977). The magnitudes of strain determined by two methods do not differ by more than 5%, on average, for the measured samples (Table 1). Orientations of the principal strains from the two methods are within a few degrees of each other. Three-dimensional strain was computed from the two-dimensional strain ratios using a modified Ramsay (1967) method (Saha 1985).

Strain magnitude and orientation

The strain ellipsoids from the Loch Skerrols thrust zone are shown in a conventional Flinn plot (Fig. 4a) and a Hsu plot (Fig. 4b) and estimates for different strain parameters are summarized in Table 2. The strain intensity (ξ_s) is higher in specimens 82, 83 and 438 close to the thrust where mylonite microstructure is obvious in thin section. The proportion of *matrix/clast* is also higher in these locations.

Table 1. Two-dimensional strain ratios estimated from quartz grain shape measurement, Loch Skerrols thrust zone. Three consecutive specimen numbers correspond to each sample location on Fig. 1(b) and refer to measurements on three mutually perpendicular sections, the third of which is sub-parallel to mesoscopic foliation. There is a close correspondence between strain ratios calculated using the two different methods

Sample No.	No. of grains measured (n)	Strain ratio from 50% data curve on R_f/ϕ plot	Strain ratio from Robin (1977) method
86.1	91	1.80	1.76
86.2	90	1.60	1.60
86.3	90	1.40	1.39
87.1	90	1.70	1.66
87.2	91	1.85	1.84
87.3	90	1.45	1.38
434 A	120	1.85	1.88
434 B	122	2.05	1.95
434 C	120	1.20	1.17
433 A	120	2.20	2.19
433 B	120	1.80	1.80
433 C	91	1.35	1.31
435 A	82	2.25	2.24
435 B	120	1.85	1.84
435 C	64	1.30	1.23
431 A	120	2.35	2.47
431 B	120	1.90	1.89
431 C	120	1.35	1.30
84.1	67	2.05	2.06
84.2	80	1.90	1.86
84.3	90	1.05	1.44
85.1	70	1.90	1.86
85.2	84	2.25	2.32
85.3	90	1.60	1.60
438 A	122	2.90	2.86
438 B	120	1.95	1.81
438 C	120	1.75	1.68
83.1	74	2.30	2.24
83.2	73	3.00	3.01
82.3	55	1.55	1.51
82.1	66	3.40	3.50
82.2	69	3.00	2.91
82.3	50	1.45	1.38

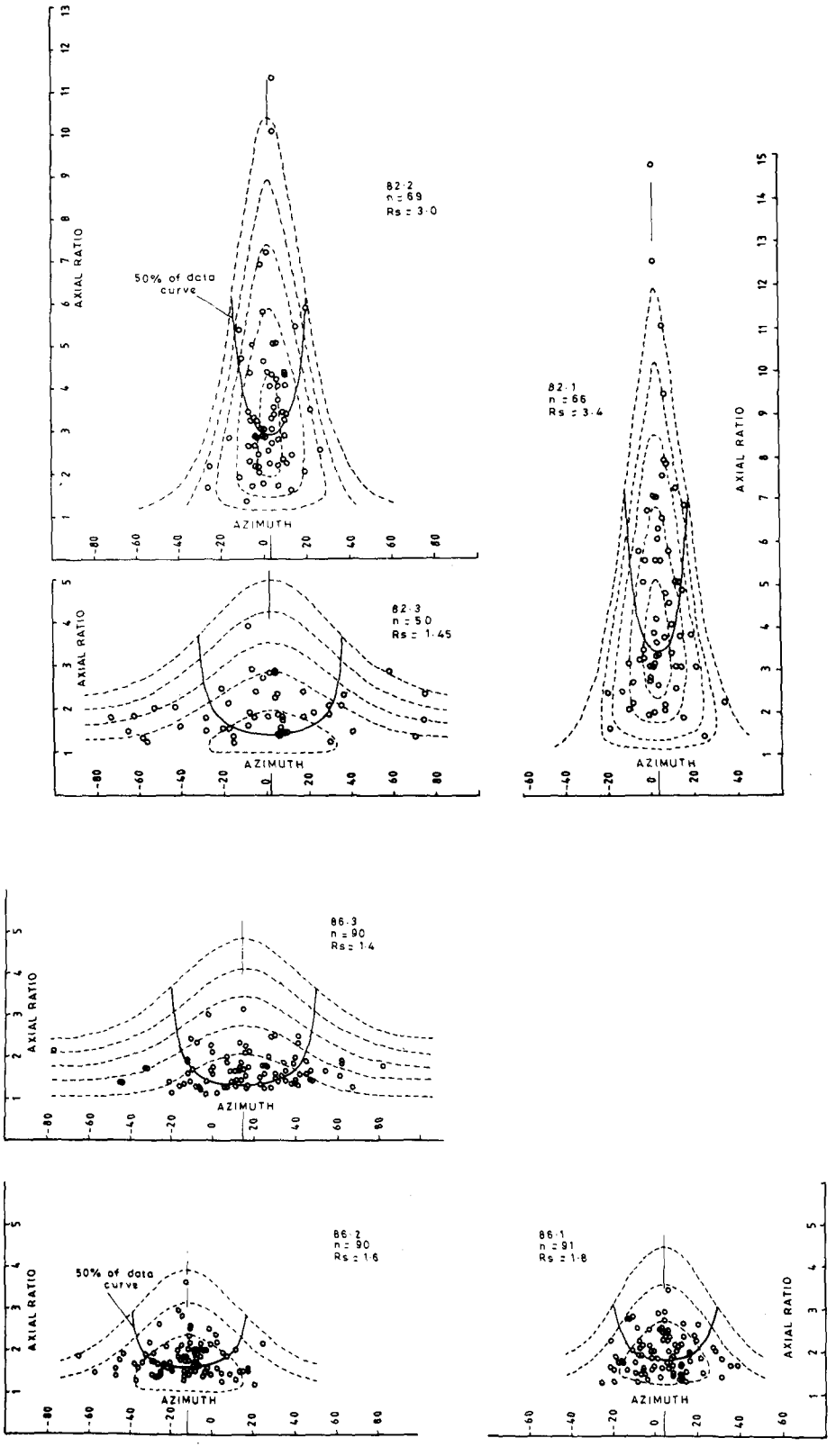

Fig. 3. Representative R_f/ϕ plots for low strain (location 86) and high strain (location 82), Loch Skerrols Thrust. For each location grain shape was measured separately on three mutually perpendicular sections: one sub-parallel to mesoscopic foliation (samples 86.3 and 82.3), a second perpendicular to foliation and lineation (samples 86.2 and 82.2) and a third perpendicular to foliation but containing the lineation (samples 86.1 and 82.1). *Rs* is the estimate of two-dimensional strain ratio from 50% of data curve shown in solid line; *n* is the number of grains measured in each sample. Dashed contours are R_f/ϕ loci for constant R_i values, starting with $R_i = 1.5$ and increments of 0.5.

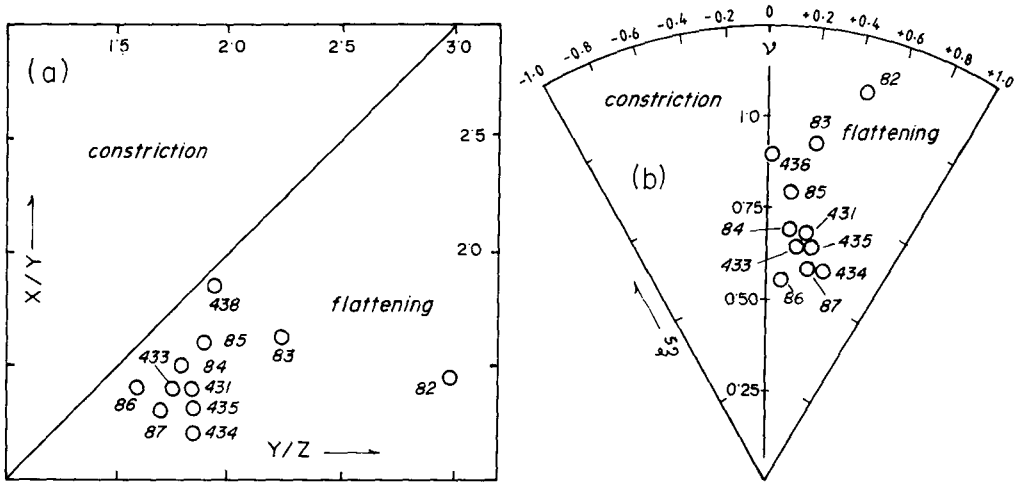

Fig. 4. Strain ellipsoids from Loch Skerrols thrust zone on (a) Flinn plot; (b) Hsu plot. Numbers refer to specimen locations given in Fig. 1(b).

It is interesting to note that although the specimens come from a thrust zone, the finite-strain ellipsoids determined from clast shape measurements fall in the apparent flattening field ($0 < k < 1, +1 > \nu > 0$), with no systematic change in k or ν towards the thrust. The question of such a shape of the finite-strain ellipsoid is discussed later.

The above strain values give only an estimate of the strain accommodated by crystal–plastic deformation in quartz clasts. It must be emphasized that these estimates are only a minimum for total strain in each locality in the thrust zone. The fine-grained matrix surrounding the clasts, which increases in volume with progressive deformation, and grain refinement are likely to accommodate relatively higher strain because of strain softening (see e.g. Tullis & Yund 1985).

The principal strain axes (X, Y, Z) show a considerable spread in orientation (Fig. 5). However, at studied locations the average XY plane is close to mesoscopic foliation (compare Figs. 2 and 5), with the X-axis subparallel to the stretching lineation. The spread in orientation of the strain axes is partly due to the sinuous course of the thrust.

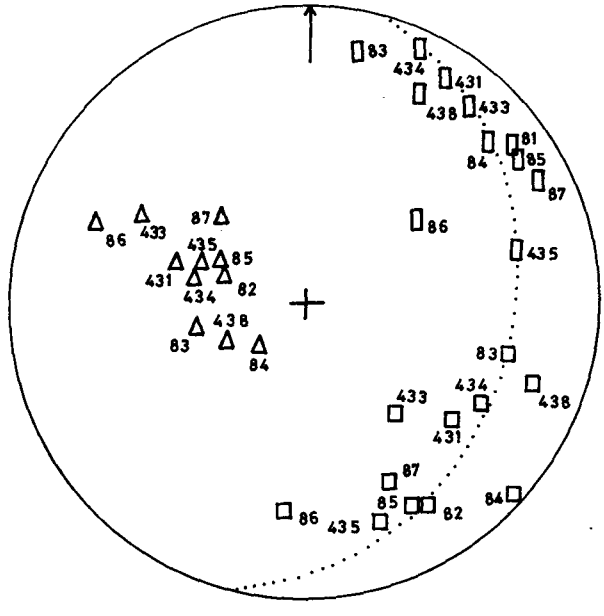

Fig. 5. Strain ellipsoid orientations in the Loch Skerrols thrust zone, equal-area plot; X—squares; Y—rectangles; Z—triangles. Numbers refer to locations in Fig. 1(b). Girdle gives the average XY plane which is close to average mesoscopic foliation. Compare with Fig. 2.

Table 2. Strain magnitudes and shapes of strain ellipsoids in the Loch Skerrols thrust zone. Specimens are arranged in order of increasing strain intensity. Specimen locations are in Fig. 1(b)

Specimen No.	Strain ellipsoid axes		Natural strains			Strain intensity	Strain ellipsoid shape	
	X/Y	Z/Y	ε_1	ε_2	ε_3	ξ_s	ν	k
86	1.4	0.6	0.37	0.04	−0.41	0.5	0.15	0.69
87	1.3	0.6	0.35	0.09	−0.44	0.6	0.34	0.42
434	1.2	0.5	0.34	0.14	−0.48	0.6	0.52	0.25
433	1.4	0.6	0.42	0.07	−0.49	0.7	0.24	0.54
435	1.3	0.5	0.39	0.11	−0.50	0.7	0.36	0.39
431	1.4	0.5	0.43	0.09	−0.52	0.7	0.30	0.47
84	1.5	0.6	0.45	0.06	−0.51	0.8	0.18	0.63
85	1.6	0.5	0.52	0.06	−0.58	0.9	0.16	0.65
438	1.9	0.5	0.64	0.02	−0.66	0.9	0.04	0.90
83	1.6	0.4	0.59	0.10	−0.69	0.9	0.25	0.50
82	1.5	0.3	0.62	0.24	−0.86	1.1	0.49	0.23

RELATIVE AGE OF THRUSTING

Islay Anticline and the Loch Skerrols Thrust

In a recent tectonic model, Colonsay and Islay are shown to lie within the Caledonian front (Fitches & Maltman 1984). In this work four phases of deformation are recognized and all post-D_1 deformation phases in the Colonsay Group are correlated with the deformation of the Dalradian sequence. The influence of flat-lying shear zones in the deformation of the frontal zone have been highlighted and the Loch Skerrols Thrust is considered a relatively higher level shear zone in this model; the inception of the Islay Anticline being approximately coincident with, and sided by the formation of, the Loch Skerrols Thrust. All these movements are interpreted to be contemporary with the generation of the D_2 structures recorded by Fitches & Maltman (1984) in the Colonsay Group (D_{1c} of Borradaile 1979). Late stages of evolution of the Islay Anticline, as well as flexing of the Loch Skerrols Thrust (sinuous course in Fig. 1), are considered to relate to D_3 structures.

Fairchild (1980) has shown the structure of NE Islay as an en échelon anticlinorium of which the Islay Anticline is an integral part. This structure is considered to represent the first phase of deformation in the area (D_{1d} of Borradaile 1979). In conventional models, the Loch Skerrols Thrust is shown to disrupt an overturned NW limb (in which the Dalradian sequence dips to the SE) of the Islay Anticline, thus accounting for the absence of stratigraphical horizons represented on the southeastern limb (e.g. Bailey 1917). The Bonahaven Formation, north of Loch Skerrols, shows a penetrative foliation, with a SE-plunging stretching lineation, comparable with that in the mylonite foliation in the Jura Quartzite close to the thrust. Minor overturned folds are also observed in the inter-bedded phyllites and impure carbonate layers in this area. However, between Crois-Mhor and Gortantoid Point [331744] (on the NW limb of Islay Anticline), the bedding in Jura Quartzite dips towards the NW. NW–SE profiles through this area should, therefore, show the Islay Anticline as an asymmetric open fold (see also Fairchild 1980). The change in style of the regional fold from south to north probably reflects the erosion level as the anticline is NE-plunging (Fitches & Maltman 1984).

Finite ellipsoid shape and strain factorization

Measurement of strain and fabric in the vicinity of Loch Skerrols shows that a definite strain gradient occurs in the area and that a significant part of the strain is accommodated by intracrystalline slip (cf. Borradaile 1979). The shape of the finite-strain ellipsoids as deduced from clast shape measurements show an apparent flattening, whereas for simple shear a plane strain ($k = 1$) finite-strain ellipsoid would be expected if the volume is unchanged during deformation. Three hypotheses may be suggested to explain the oblate shape of the finite-strain ellipsoid:

(i) there was differential volume loss during deformation across the thrust;

(ii) a later deformation (D_{2d}?) following thrust movement changed the shape of a plane strain ellipsoid associated with thrust movement;

(iii) the observed finite-strain ellipsoid is due to the combined effect of an initial constrictive or flattening deformation related to D_{1d} plus a plane strain type deformation related to thrust movement.

Figure 6 shows the field in which the observed strain ellipsoids lie; the boundary between the constrictive and flattening field for different volume loss are also shown. Since the observed strain field crosses lines for different volume loss, the overall deformation could only be regarded as plane strain if accompanied by different amounts of volume loss at different specimen localities. In view of the similar lithology and deformation mechanism throughout the thrust zone, the proposition of different volume loss seems geologically unrealistic. Thus the hypothesis (i) above is rejected.

Minor crenulations and kinks on schistosity in NE Islay show that a phase of deformation (D_{2d} of Borradaile; D_4 of Fitches & Maltman) post-dates the thrust movement. However, the effect is only local and is not penetrative enough to produce changes of shape on a grain scale. Thus D_{2d} is considered to have negligible effect on the finite-strain ellipsoid.

A penetrative axial plane cleavage is associated with the Islay Anticline (D_{1d}). Borradaile (1979) recorded both constrictional and flattening strain from various Dalradian horizons on either limb of the Islay Anticline. An intragranular component of D_{1d} strain must have had some imprint on the Jura Quartzite which is also deformed in the Loch Skerrols thrust zone. Between Loch Cam [345665] and Loch Skerrols, the thrust zone foliation strikes parallel to that of the axial plane cleavage recorded farther east (Fairchild 1980); however, the thrust zone foliation is more gently inclined.

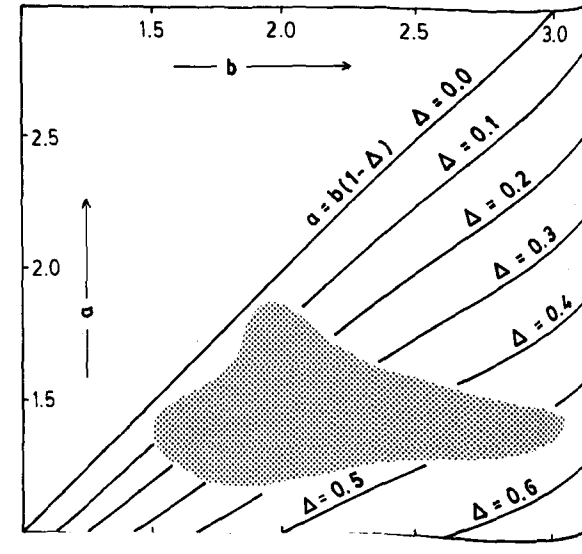

Fig. 6. Field of observed strain ellipsoids in the Loch Skerrols thrust zone (data of Fig. 5) and its relationship with the boundary between constriction and flattening strain for different amounts of volume loss (Δ).

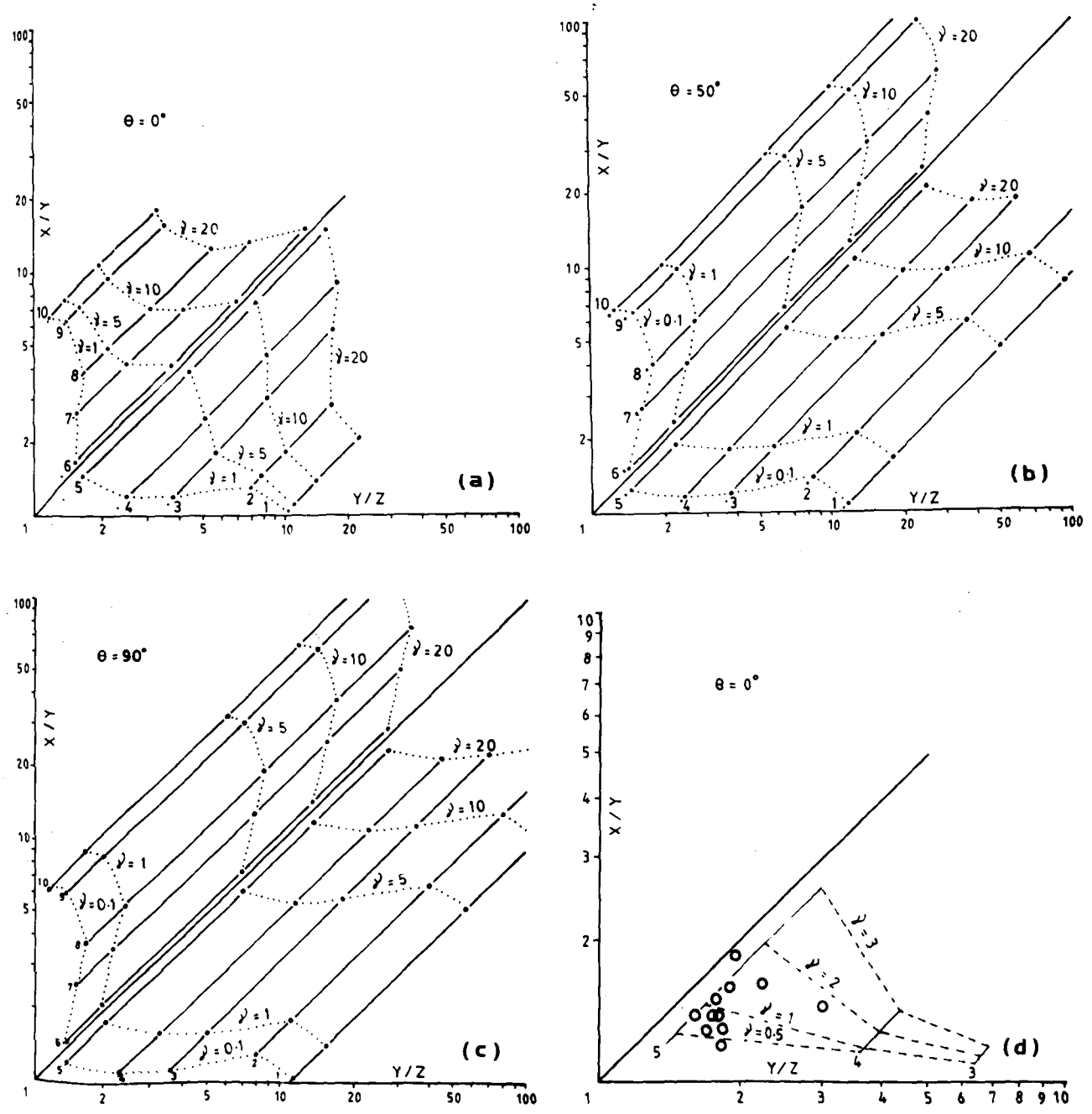

Fig. 7. Flinn diagram showing solutions to deformation gradient tensor for a strain superposition model (pre-multiplication by simple shear of prolate or oblate strain) taking into consideration varying obliquities (θ) of the shear-zone boundary with respect to the *pre-thrusting XY* plane. See text and the Appendix for details. Strain paths corresponding to five prolate and five oblate *pre-thrusting* strain ellipsoids are shown for γ values up to 20. (a) $\theta = 0°$ case; (b) $\theta = 50°$ case; (c) $\theta = 90°$ case; (d) an attempt to model the strain field of the Loch Skerrols thrust zone; $\theta = 0°$ case. Pre-thrusting ellipsoids are numbered 1–10 with k values 0.001, 0.043, 0.056, 0.073, 0.499 (oblate ones), 1.243, 2.804, 4.068, 12.375, 28.725 (prolate ones), respectively.

Presuming that the thrust developed after considerable amplification of the Islay Anticline, the influence of the 'initial' shape of the strain ellipsoid on the final shape is evaluated in a strain superposition model.

In this model a simple shear deformation is considered to be operative during thrusting. Constancy of the intermediate principal strain axis (Y) throughout this deformation and equivoluminal strain are assumed. The model takes into account varying obliquity of the shear direction with respect to pre-thrusting orientation of maximum principal strain axis; assuming that at an intermediate stage XY plane of strain ellipsoid is close to axial plane cleavage orientation, the obliquity refers to the then angle between axial plane cleavage and shear-zone boundary (also shear direction).

The algebra involved in the computation is given in the Appendix and is essentially similar to that used in an earlier model of strain variation in thrust zones (Sanderson 1976). The results demonstrate that even for very high shear strains ($\gamma = 20$) the strain path does not cross the plane strain line on a Flinn plot (Fig. 7); the final ellipsoid shape is constrictional or flattened depend-

RELATIVE AGE OF THRUSTING

Islay Anticline and the Loch Skerrols Thrust

In a recent tectonic model, Colonsay and Islay are shown to lie within the Caledonian front (Fitches & Maltman 1984). In this work four phases of deformation are recognized and all post-D_1 deformation phases in the Colonsay Group are correlated with the deformation of the Dalradian sequence. The influence of flat-lying shear zones in the deformation of the frontal zone have been highlighted and the Loch Skerrols Thrust is considered a relatively higher level shear zone in this model; the inception of the Islay Anticline being approximately coincident with, and sided by the formation of, the Loch Skerrols Thrust. All these movements are interpreted to be contemporary with the generation of the D_2 structures recorded by Fitches & Maltman (1984) in the Colonsay Group (D_{1c} of Borradaile 1979). Late stages of evolution of the Islay Anticline, as well as flexing of the Loch Skerrols Thrust (sinuous course in Fig. 1), are considered to relate to D_3 structures.

Fairchild (1980) has shown the structure of NE Islay as an en échelon anticlinorium of which the Islay Anticline is an integral part. This structure is considered to represent the first phase of deformation in the area (D_{1d} of Borradaile 1979). In conventional models, the Loch Skerrols Thrust is shown to disrupt an overturned NW limb (in which the Dalradian sequence dips to the SE) of the Islay Anticline, thus accounting for the absence of stratigraphical horizons represented on the southeastern limb (e.g. Bailey 1917). The Bonahaven Formation, north of Loch Skerrols, shows a penetrative foliation, with a SE-plunging stretching lineation, comparable with that in the mylonite foliation in the Jura Quartzite close to the thrust. Minor overturned folds are also observed in the inter-bedded phyllites and impure carbonate layers in this area. However, between Crois-Mhor and Gortantoid Point [331744] (on the NW limb of Islay Anticline), the bedding in Jura Quartzite dips towards the NW. NW–SE profiles through this area should, therefore, show the Islay Anticline as an asymmetric open fold (see also Fairchild 1980). The change in style of the regional fold from south to north probably reflects the erosion level as the anticline is NE-plunging (Fitches & Maltman 1984).

Finite ellipsoid shape and strain factorization

Measurement of strain and fabric in the vicinity of Loch Skerrols shows that a definite strain gradient occurs in the area and that a significant part of the strain is accommodated by intracrystalline slip (cf. Borradaile 1979). The shape of the finite-strain ellipsoids as deduced from clast shape measurements show an apparent flattening, whereas for simple shear a plane strain ($k = 1$) finite-strain ellipsoid would be expected if the volume is unchanged during deformation. Three hypotheses may be suggested to explain the oblate shape of the finite-strain ellipsoid:

(i) there was differential volume loss during deformation across the thrust;

(ii) a later deformation (D_{2d}?) following thrust movement changed the shape of a plane strain ellipsoid associated with thrust movement;

(iii) the observed finite-strain ellipsoid is due to the combined effect of an initial constrictive or flattening deformation related to D_{1d} plus a plane strain type deformation related to thrust movement.

Figure 6 shows the field in which the observed strain ellipsoids lie; the boundary between the constrictive and flattening field for different volume loss are also shown. Since the observed strain field crosses lines for different volume loss, the overall deformation could only be regarded as plane strain if accompanied by different amounts of volume loss at different specimen localities. In view of the similar lithology and deformation mechanism throughout the thrust zone, the proposition of different volume loss seems geologically unrealistic. Thus the hypothesis (i) above is rejected.

Minor crenulations and kinks on schistosity in NE Islay show that a phase of deformation (D_{2d} of Borradaile; D_4 of Fitches & Maltman) post-dates the thrust movement. However, the effect is only local and is not penetrative enough to produce changes of shape on a grain scale. Thus D_{2d} is considered to have negligible effect on the finite-strain ellipsoid.

A penetrative axial plane cleavage is associated with the Islay Anticline (D_{1d}). Borradaile (1979) recorded both constrictional and flattening strain from various Dalradian horizons on either limb of the Islay Anticline. An intragranular component of D_{1d} strain must have had some imprint on the Jura Quartzite which is also deformed in the Loch Skerrols thrust zone. Between Loch Cam [345665] and Loch Skerrols, the thrust zone foliation strikes parallel to that of the axial plane cleavage recorded farther east (Fairchild 1980); however, the thrust zone foliation is more gently inclined.

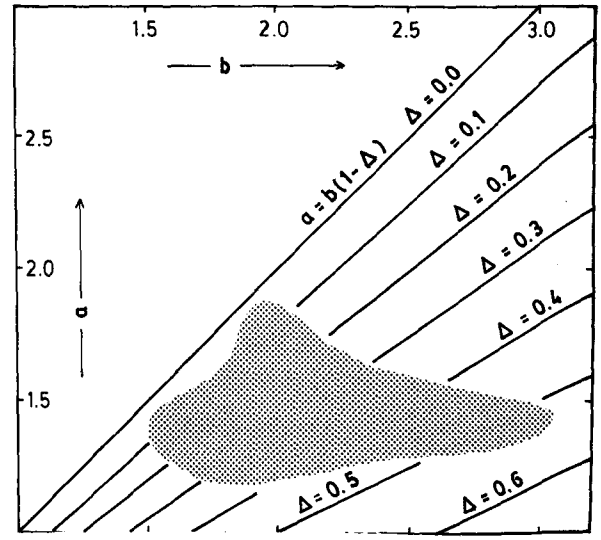

Fig. 6. Field of observed strain ellipsoids in the Loch Skerrols thrust zone (data of Fig. 5) and its relationship with the boundary between constriction and flattening strain for different amounts of volume loss (Δ).

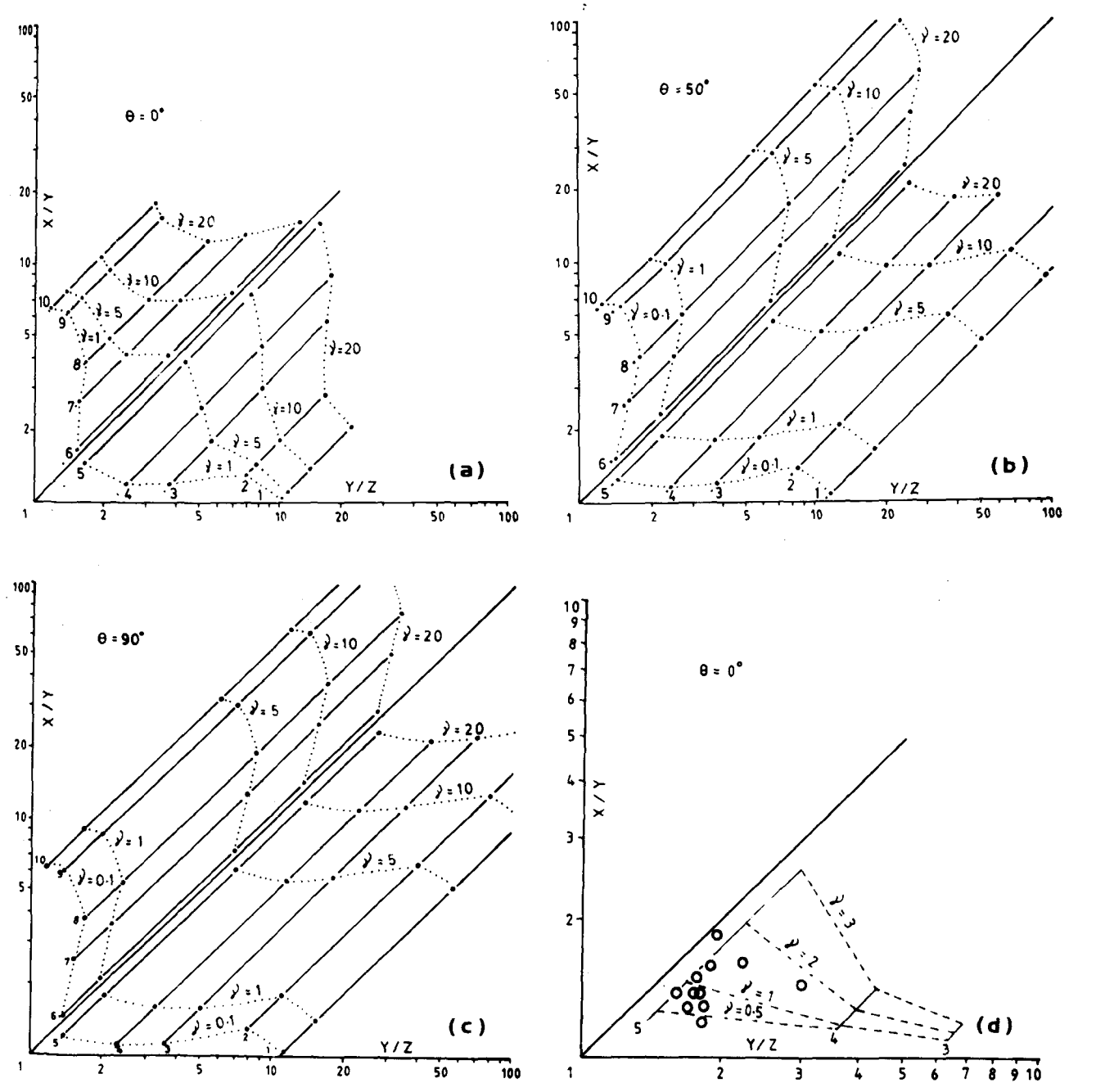

Fig. 7. Flinn diagram showing solutions to deformation gradient tensor for a strain superposition model (pre-multiplication by simple shear of prolate or oblate strain) taking into consideration varying obliquities (θ) of the shear-zone boundary with respect to the *pre-thrusting XY* plane. See text and the Appendix for details. Strain paths corresponding to five prolate and five oblate *pre-thrusting* strain ellipsoids are shown for γ values up to 20. (a) $\theta = 0°$ case; (b) $\theta = 50°$ case; (c) $\theta = 90°$ case; (d) an attempt to model the strain field of the Loch Skerrols thrust zone; $\theta = 0°$ case. Pre-thrusting ellipsoids are numbered 1–10 with k values 0.001, 0.043, 0.056, 0.073, 0.499 (oblate ones), 1.243, 2.804, 4.068, 12.375, 28.725 (prolate ones), respectively.

Presuming that the thrust developed after considerable amplification of the Islay Anticline, the influence of the 'initial' shape of the strain ellipsoid on the final shape is evaluated in a strain superposition model.

In this model a simple shear deformation is considered to be operative during thrusting. Constancy of the intermediate principal strain axis (Y) throughout this deformation and equivoluminal strain are assumed. The model takes into account varying obliquity of the shear direction with respect to pre-thrusting orientation of maximum principal strain axis; assuming that at an intermediate stage XY plane of strain ellipsoid is close to axial plane cleavage orientation, the obliquity refers to the then angle between axial plane cleavage and shear-zone boundary (also shear direction).

The algebra involved in the computation is given in the Appendix and is essentially similar to that used in an earlier model of strain variation in thrust zones (Sanderson 1976). The results demonstrate that even for very high shear strains ($\gamma = 20$) the strain path does not cross the plane strain line on a Flinn plot (Fig. 7); the final ellipsoid shape is constrictional or flattened depend-

ing on whether the pre-thrusting strain ellipsoid is in the constriction or flattening field, respectively. The general field to which the final ellipsoid shape belongs is also independent of the obliquity (θ) of the shear direction (compare Figs. 7a, b & c which are for $\theta = 0°$, $\theta = 50°$ and $\theta = 90°$, respectively). The above strain factorization gives an estimate of γ between 0.5 and 2 (Fig. 7d).

A possible sequence of evolution of the Islay Anticline is shown schematically in Fig. 8. The two different final profiles (Fig. 8c) correspond to an ESE–WNW section through Loch Skerrols (on the right) and a section farther north through Gortantoid point in NW Islay (on the left). The change in shape of the fold profile may be due to: (a) level of erosion; (b) divergence of the movement zone from the trend of the major fold axis; or (c) dissipation of the movement along one or more slides without any significant drag effect on the NW limb. The analysis above favours the suggestion that the Loch Skerrols Thrust post-dates a stage of considerable amplification (but not much tightening) of the Islay Anticline. Thus the structure is considered to be comparable with a break thrust (quoted in Willis 1894, House & Gray 1982).

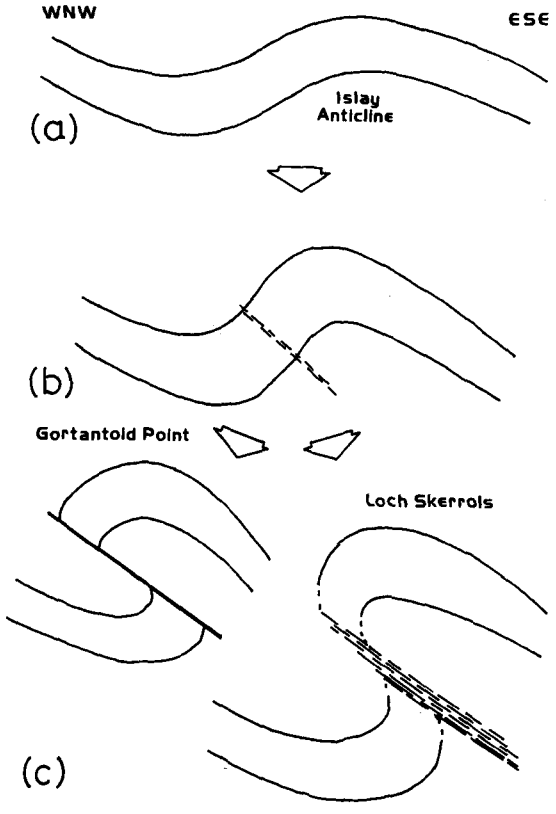

Fig. 8. Schematic sketches showing the evolution of the Islay Anticline with progressive deformation. The Loch Skerrols Thrust transgressed the western limb after considerable amplification of the anticline (stage b). Two alternative paths from stage (b) reflect observed differences in fold profile between Loch Skerrols and Gortantoid Point (NW Islay). Note that the footwall syncline shown here has not been mapped in the area.

MICROSTRUCTURAL VARIATION IN A ZONE OF STRAIN GRADIENT

Microstructure

As shown earlier, the traverse from Loch Cam to a point 0.5 km north of Knockdon Farm reveals a zone of natural strain gradient across Loch Skerrols thrust zone. The microstructural evolution of the Jura Quartzite associated with the thrust has been studied in samples collected at varying distances from the western boundary of the Jura Quartzite (sample locations in Fig. 1b). The Loch Skerrols Thrust separates the Bowmore Sandstone and Jura Quartzite, but contact between the two units is not exposed in the An Carn–Knockdon area. Changes in optical microstructure with increasing strain are illustrated in Figs. 9(a)–(e). In the following discussion *matrix* refers to aggregate of small grains (30–50 μm) surrounding porphyroclasts of larger grains ($\geq$0.5 mm). The larger grains are deformed sedimentary grains and are considered to be *clasts*. As described below the *clasts* contribute to the *matrix* through dynamic recrystallization and attendant grain refinement. The term dynamic recrystallization is used here to indicate grain-boundary migration-accommodated recovery during dislocation creep (Tullis & Yund 1985). Only optical microstructures form the basis of any inference drawn here.

At an overall strain intensity, $\xi_s \approx 0.55$, the quartz clasts show undulose extinction, deformation bands (Fig. 9d) and small recrystallized grains are generally restricted to clast boundaries producing a core and mantle structure (White 1976). Although the samples studied contain $\leq$1% feldspar, twin lamellae in feldspar grains are diffuse and some of these clasts show pull-aparts.

With increasing strain ($\xi_s \approx 0.8$) the proportion of *matrix* to *clast* increases (Fig. 9b). The recrystallized grains have straight to gently curved boundaries, except where they occur at the boundary of a relict porphyroclast core, in which case, lobate grains can be seen. Some of the larger clasts are broken down into sub-parallel ribbon grains separated by trails of recrystallized grains, which show a weak shape fabric sub-parallel to the mylonitic foliation.

At the highest recorded strain intensity ($\xi_s \approx 1.1$), the proportion of matrix grains is more than 85% (Fig. 9c). Recrystallization of highly elongated clasts is common (Fig. 9e), producing generally straight grain boundaries, often aligned parallel to each other, thus defining the mylonite foliation. Some recrystallized grains are larger than average probably due to static grain growth.

The proportion of *matrix/clast* increases with increasing strain, the relative proportion of sericite is also higher in specimens with higher strain. The latter is interpreted as a transformation of kaolinized feldspar to micaceous minerals. However, the average size of recrystallized grains does not show much variation (Table 3). The frequency distribution of the aspect ratio of recrystallized grains also maintains the same general

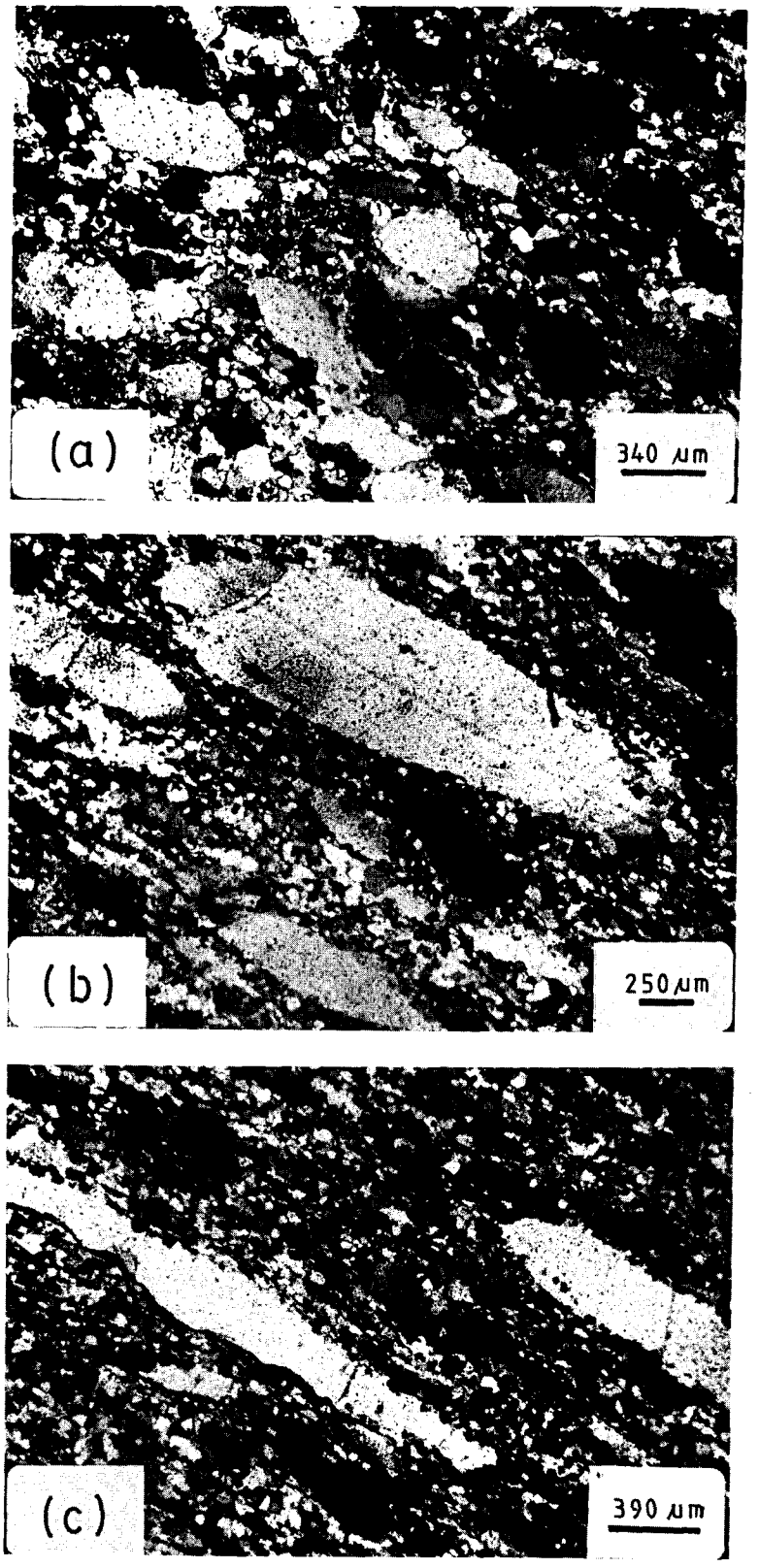

Fig. 9. Microstructural changes in Jura Quartzite in the vicinity of Loch Skerrols Thrust. Photomicrographs from sections cut perpendicular to foliation but parallel to lineation, except (a) where the section is perpendicular to lineation. (a) Flattening of clasts is minimum, *matrix* to *clast* ratio is only 0.54, location 87. (b) *Clasts* are more flattened, location 85. (c) Highly elongated *clasts*; proportion of *matrix* is also higher (85%), location 82. (*Continued.*)

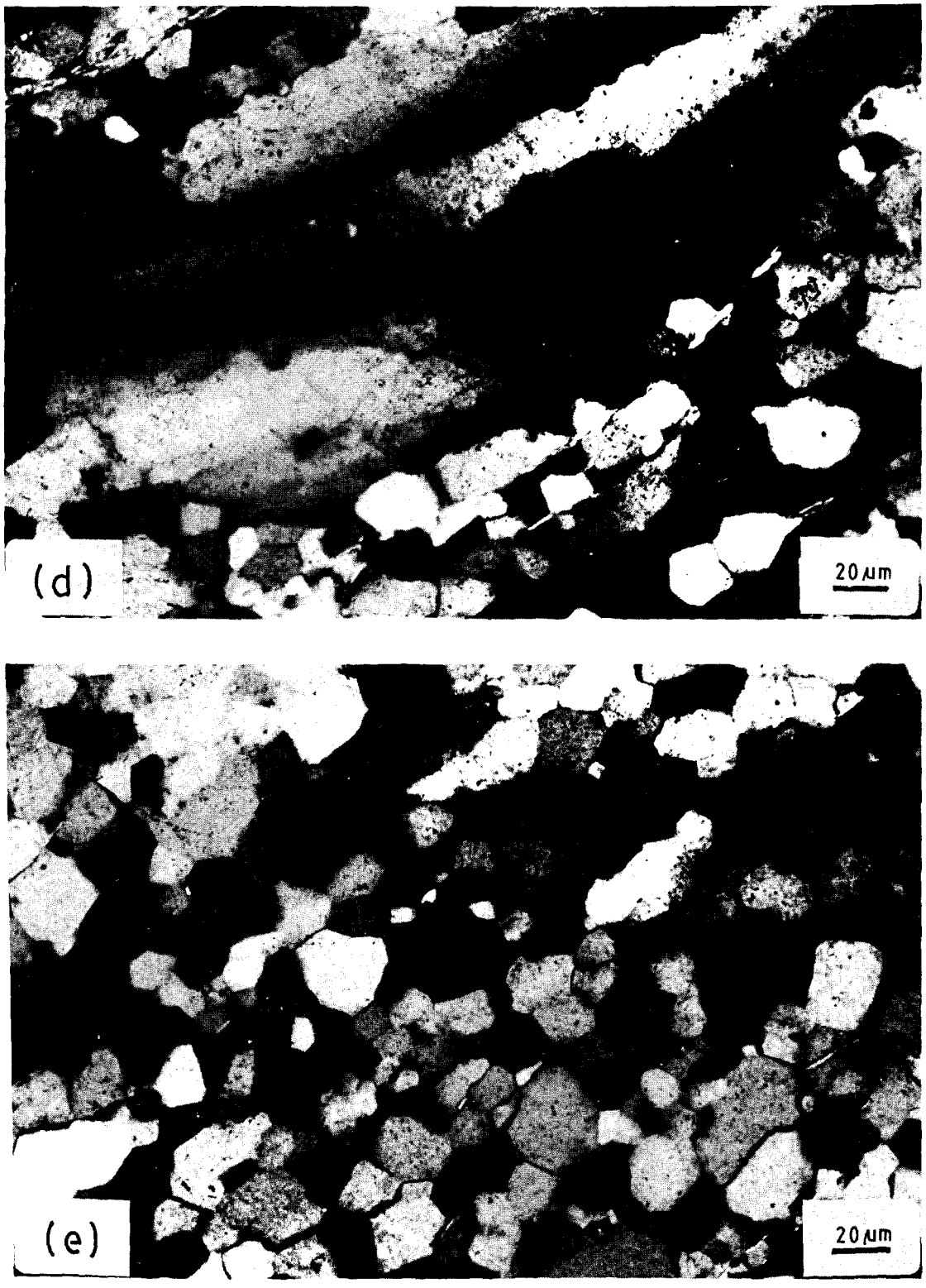

Fig. 9. *Continued.* (d) At lower strain ($X/Z < 2$) dynamic recrystallization is more commonly restricted to grain boundaries, location 86. (e) At higher strains ($X/Y < 4$–6) thorough recrystallization of quartz *clasts* occur; recrystallized grain boundaries are also aligned, location 83.

Table 3. Recrystallized quartz grain size and palaeostress estimates from Loch Skerrols thrust zone. Specimens are arranged in order of increasing strain intensity, ξ_s. Specimen locations are in Fig. 1. Flow stresses are calculated using equations: I. Twiss (1977) $\sigma = 603\,(D_j)^{-0.68}$; II. Mercier *et al.* (1977) $\sigma = 381\,(D_j)^{-0.71}$; III. Ord & Christie (1984) $\sigma = 4090\,(D_j)^{-1.11}$, D_j is average grain diameter, for details of calculation see text

Specimen No.	Matrix proportion (%)	Recrystallized grain size ($D_j \pm$ S.D.)	Palaeostress (MPa) I	II	III
86	50	32 ± 16	57	33	87
87	54	26 ± 11	66	38	110
84	55	30 ± 11	60	34	94
85	55	28 ± 10	63	36	101
83	80	33 ± 15	56	32	84
82	85	33 ± 17	56	32	84

pattern irrespective of strain value (Fig. 10). The modal class in both low and high strain samples includes grains with an aspect ratio between 1 and 2. These may be interpreted as due to either a post-tectonic static recrystallization, or a dynamic recrystallization attained through grain-boundary-migration accommodated recovery. In the latter case, cyclic slip and recrystallization during progressive deformation prevents survival of early recrystallized grains with high dislocation density, i.e. highly flattened early fine grains are dispensed with (Tullis & Yund 1985).

Both in low and high strain samples the recrystallized grains originating from a single clast (relict outline defined by mica trails) show a relatively high neighbour mismatch, misorientation angle being >10° in more than 80% of cases; the modal misorientation angle is around 30° in low strain samples and around 15° in high strain samples. A quartz–(feldspar)–chlorite–sericite mineral paragenesis prevails throughout the thrust zone and as such there is little difference in thermal influence between low and high strain samples. In such a situation, any post-tectonic static recrystallization will have to be driven mostly by differences in strain energy. Sub-grain controlled nucleation and subsequent grain-boundary migration during static recrystallization (Nicolas & Poirier 1976) would have entailed more frequent low angle (<10°) boundaries. Recrystallization due to progressive sub-grain rotation (dislocation climb assisted recovery of Tullis & Yund 1985) would also have been expected to produce more frequent low-angle boundaries between neighbours, especially at low strains. Microstructural development in the Loch Skerrols thrust zone is thus considered to be largely controlled by a grain-boundary migration-accom-

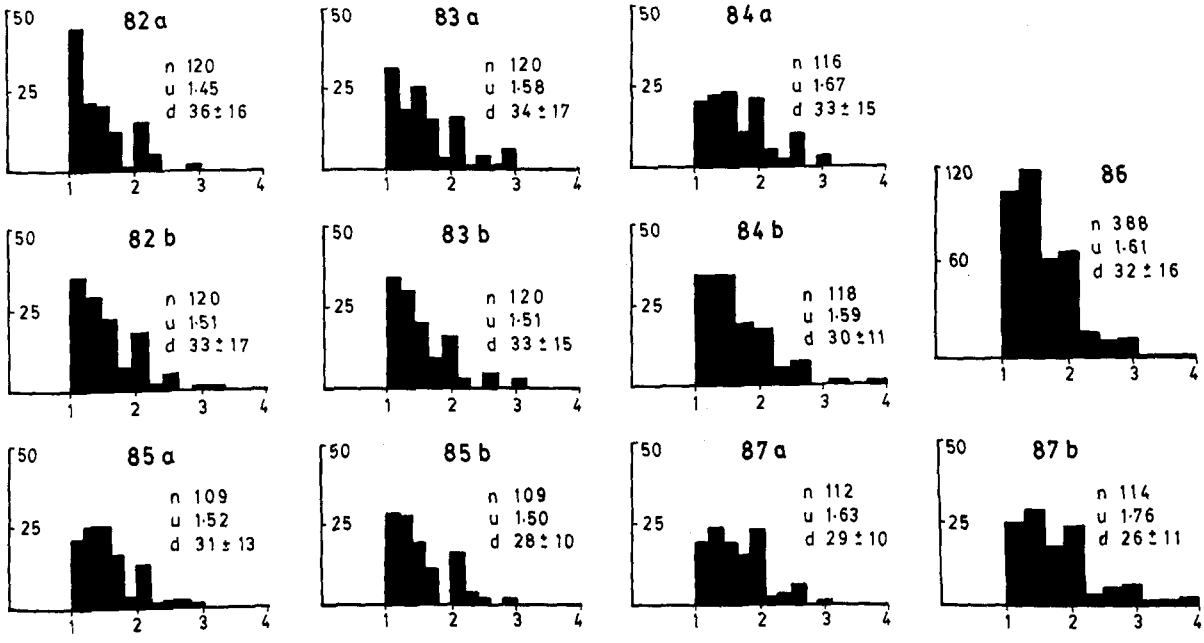

Fig. 10. Frequency distribution of the aspect ratio of dynamically recrystallized grains in specimens with different strain intensities. Strain values generally decrease from specimen locations 82–87. The mean aspect ratio (μ) shows little change with strain; d is average grain intercept (±1 S. D.) in microns; n is the number of grains measured in each thin section. a and b with each specimen location number refer to two mutually perpendicular thin sections cut perpendicular to foliation, but one parallel, the other normal, to lineation, from each specimen. For location 86 only perpendicular to lineation section is measured.

modated recrystallization with progressive deformation. As presented in a later section, better defined preferred orientation of recrystallized grains in high strain samples is also consistent with cyclic slip and recrystallization.

Palaeostress estimate

Deformation-induced dislocation density, sub-grain size and dynamically recrystallized grain size in rocks from deeply eroded fault zones may provide signatures of differential stress that existed when the fault was active (Nicolas & Poirier 1976, Mercier *et al.* 1977, Twiss 1977, Weathers *et al.* 1979, White 1979, Christie & Ord 1980, Kohlstedt & Weathers 1980, Schmid 1980, Ord & Christie 1984). Theoretical arguments and experimental observations demonstrate that the microstructural elements, if generated during steady-state deformation, will depend primarily on the flow stress (Mercier *et al.* 1977, Twiss 1977). Although the principle has been applied by a number of workers (e.g. Twiss 1977, Burg & Laurent 1978, Etheridge & Wilkie 1979, Weathers *et al.* 1979, White 1979, Christie & Ord 1980, Ord & Christie 1984), uncertainties exist in the derivation of flow stresses from microstructural information (discussions in Ord & Christie 1984). In particular, presence of mica or other impurity phases limit the grain size by impeding the boundaries of quartz grains during growth (Hobbs *et al.* 1976). Recrystallized grain sizes may also be related to a variation in chemical environment with constant flow stress. For a given flow stress different recrystallized grain sizes have been observed in samples of experimentally deformed quartzite under 'wet' and 'dry' conditions, which suggests the possibility of an influence of water content on the dynamic relationship between grain size and stress (Christie *et al.* 1980). Annealing recovery/recrystallization may also substantially alter microstructures attained during syntectonic recrystallization (e.g. Ord & Christie 1984).

In the present case only recrystallized grain size in samples of deformed Jura Quartzite from the Loch Skerrols thrust zone is used in estimating the flow stress. Since, the mineral paragenesis in the thrust zone indicates only a lower-greenschist facies *PT* environment, the influence of annealing recovery is thought to be minimal. Care has been taken to select mica free areas for grain size measurement in thin sections of Jura Quartzite. Mutually perpendicular longest and shortest intercepts (D_{i1} and D_{i2}) on each grain were measured under an optical microscope (magnifications up to ×400) and using a micrometer ocular. Grain size (D) is calculated using the formula,

$$D = 1/n \sum_{i=1}^{n} (D_{i1}D_{i2})^{1/2},$$

where n is the number grains measured; $n \geqslant 210$ in each sample. Since the recrystallized grains have small aspect ratios (Fig. 10) the method adopted here for grain size measurement is believed to approximate results obtainable from a method using linear intercepts (Smith & Guttman 1953). The results of flow stress calculations are shown in Table 3 and the salient points are discussed below.

Although the proportion of *matrix/clast* increases with increasing strain, the average size of recrystallized grains does not show much variation (26–33 μm). The average value of the palaeostresses in the Loch Skerrols thrust zone using the Twiss method is 60 MPa which compares well with values of 50–130 MPa obtained for the Moine thrust zone (Christie 1963, Twiss 1977). A southward decrease in the flow stress value has been reported for the Moine thrust zone near Knockan Crag, Stack of Glencoul and the Loch Eriboll area (Weathers *et al.* 1979, Ord & Christie 1984). Coincidentally, the flow stress estimates for the Loch Skerrols Thrust, which Kennedy (1946) suggested to be an extension of the Moine Thrust, is at the lower end of the range of values given by different workers for the Moine thrust zone. Comparable magnitudes of flow stress from quartz grain-size palaeopiezometry have been estimated from other shear zones where a crystal–plastic deformation mechanism prevailed (Twiss 1977, White 1979, Kohlstedt & Weathers 1980).

QUARTZ *c*-AXIS FABRIC

Fabric measurement and representation

The specimens used for fabric measurement were those used for strain determinations. Quartz *c*-axes were measured by standard universal stage techniques (Fairbairn 1949, Turner & Weiss 1963) for each of two mutually perpendicular thin sections. Necessary rotations were implemented before comparing fabric diagrams obtained from separate thin sections. Parts of the thin section containing a relatively high proportion of mica were avoided so that we are dealing essentially with a monomineralic fabric. The results for *matrix* grains are shown in Fig. 11. Orientations of quartz *c*-axes in *clasts* were plotted separately (Fig. 12). Separate measurements were taken for different subgrains, deformation bands and recrystallized grains within a single clast.

The fabric pattern

Matrix. For low strain value locations (Fig. 11—434, 87, 86 and 84) the fabric pattern is rather diffuse. However, the equatorial plane (close to *XZ* plane) contains one or more point-maximum (2–3 × *E*) that are closer to *Z* than to *X*. The foliation plane and *XY* plane show very low concentrations of *c*-axes. With higher strain intensity (locations 85 and 83) a weak cross-girdle pattern appears. The better developed girdle with point-maximum (3–4 × *E*) near foliation normal (*Z*) passes through *Y*. In specimen 83 there is a sub-maximum near *Y*. In highly deformed specimens (locations 82 and 438) the fabric pattern is close to the type-I cross girdle (Lister & Williams 1979) with point-maximum (3–5 × *E*) on the *XZ* plane; the angle between the point-maximum

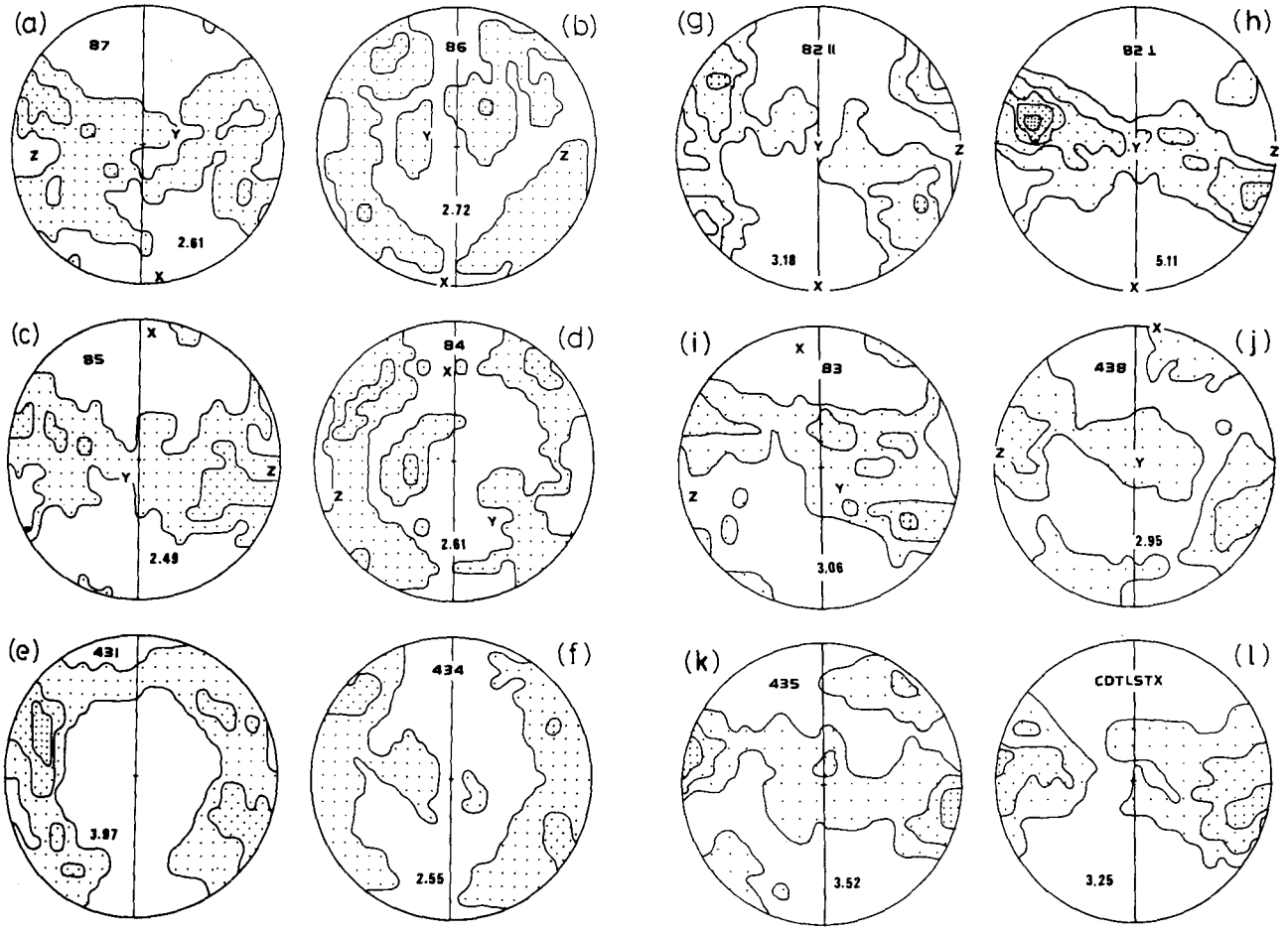

Fig. 11. Quartz *c*-axis fabric (*matrix* grains) for different specimens in Loch Skerrols thrust zone. Specimen numbers are given as bold figures in the upper part of each diagram. Lower-hemisphere equal-area plots contoured in multiples of E, expectation for uniform distribution. The maximum point density ($\times E$) is given in the lower part of each diagram. Foliation trace runs N–S; structural top of foliation is towards east. X, Y, Z refer to relative orientations of principal strains. 400 measurements in each thin section.

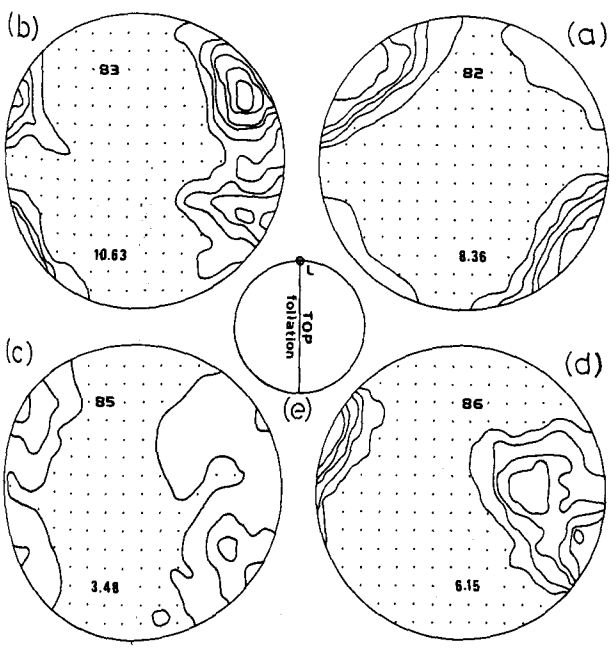

Fig. 12. Quartz *c*-axis fabric for *clast* grains. The relative orientations of foliation, lineation and structural top in all the diagrams (a–d) are as in (e). For other details see the legend in Fig. 11.

and Z is less than 20°. The fabric pattern is marked by an internal asymmetry : a main girdle with minor girdles branching off (Figs. 11g–k).

For specimen CDTLSTX (Fig. 11l) which comes from the Bun-an-Uillt area, strain data are not available. Microstructurally it resembles a mylonite with a very high proportion of *matrix* grains. The fabric pattern shows an incomplete single girdle with point maximum ($3 \times E$) subnormal to the foliation (Fig. 11l). The angle between foliation normal and the point-maximum is about 15°, the offset being in the same senses as that for the main girdle at location 82.

Clasts. The essential pattern for *clast* *c*-axes is a paired maximum with unequal development of the two concentrations lying on the equatorial plane, perpendicular to the foliation (Fig. 12). In the most deformed specimen (location 82) the stronger cluster is in a position comparable to that of the main girdle in the matrix fabric. A similar pattern is obtained for location 85, and in location 86 there is a maximum only on one side of the foliation normal (Z). The fabric corresponding to location 83 shows clusters on either side of the foliation normal, but the stronger cluster (point-maximum : 8–10 $\times E$) is disposed in a sense opposite to that for all other samples.

A number of measurements for *c*-axis orientation were made on the same clast to account for different sub-grain orientations or deformation bands. The number varied from five in the less deformed specimen 86 to 50 in the more deformed specimens 83 and 82. Thus the effective sample size is smaller than in the corresponding matrix fabric and the much higher point-maximum (10–11 × *E*) in these fabric diagrams may reflect the influence of host-grain control.

Discussion. The essential pattern of quartz *c*-axis fabric in matrix grains is a type-I cross girdle which becomes well defined with increasing strain in the Loch Skerrols thrust zone. The pattern is asymmetric, both internally and with respect to the foliation, lineation and the *X, Y, Z* finite-strain axes in more deformed specimens. Fabric asymmetry criteria for determining the sense of vorticity have been discussed and applied by a number of workers (e.g. Bouchez & Pêcher 1976, Berthé *et al.* 1979, Lister & Williams 1979, Brunel 1980, Lister & Hobbs 1980, Simpson 1980, Passchier 1983, Simpson & Schmid 1983). The quartz *c*-axis fabric patterns in the Loch Skerrols thrust zone indicate a dextral sense of movement in Fig. 11. Reorientation of the foliation and lineation to their true geographic position makes the sense of movement consistent with a westward movement of the Dalradian over the Bowmore Sandstone along the Loch Skerrols Thrust (Fig. 13). Although the clast fabric at location 83 shows an opposite sense of shear, the unequal development of the two maxima in diagrams corresponding to locations 82, 85 and 86 is consistent with the sense of shear determined from the better defined matrix fabric.

The external asymmetry of the observed fabric pattern is a reflection of the non-coaxial deformation along the Loch Skerrols Thrust. Assuming a steady-state deformation and that grains are oriented for easy slip during strain-induced fabric development, the point-maximum close to *Z*, could be due to a dominant activity of the basal ⟨*a*⟩ slip system (Tullis *et al.* 1973, Bouchez *et al.* 1983). This is consistent with the temperature conditions deduced from a mineral paragenesis of chlorite + sericite + quartz. However, a girdle pattern for the matrix fabric indicates more than one operative slip system. To explain concentrations near *Y* and intermediate positions glide on other slip systems is required, e.g. prism ⟨*a*⟩ or dipyramid ⟨*a* + *c*⟩.

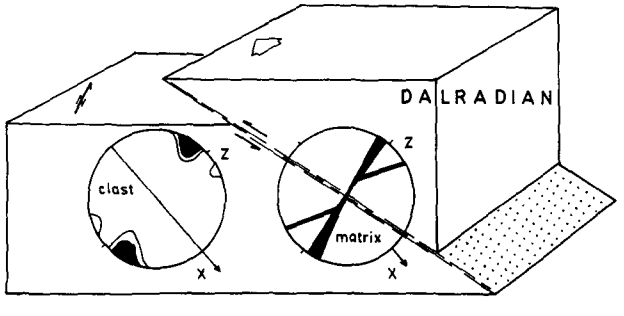

Fig. 13. Movement along Loch Skerrols Thrust and its relation with asymmetry of quartz *c*-axis fabric. Idealized block diagram to show the westerly movement of the Dalradian 'block'. The fabric skeletons in mylonitized Jura Quartzite (both *matrix* and *clast*) in their true geographic orientation on an ESE–WNW section are shown. Note that a better developed girdle in *matrix* fabric is normal to the thrust plane.

CONCLUSIONS

The component of finite strain accommodated by crystal-plastic deformation increases towards the western boundary of the Jura Quartzite in the Loch Skerrols thrust zone. The maximum observed value of the intracrystalline strain is given by the strain ratio 1.9:1.3:0.4, $\xi_s = 1.1$. The *X*-axis of the finite-strain ellipsoid is close to the stretching lineation in quartz mylonites, the foliation plane being sub-parallel to the *XY* plane. Microstructural changes with increasing strain are reflected in the increasing *matrix/clast* ratio and better defined fabric pattern at higher strain, which are interpreted in terms of cyclic slip and grain boundary migration accommodated recrystallization. Palaeostress estimates from the size of recrystallized quartz grains in the Loch Skerrols thrust zone indicate a differential stress of ~60 MPa, comparable to the stress magnitude obtained from the Moine thrust zone in the Loch Eriboll area (see Weathers *et al.* 1979).

At higher strains the quartz *c*-axis fabric is a type-I cross girdle pattern with an asymmetry reflecting non-coaxial deformation and westward transport of the Dalradian block over the Bowmore Sandstone along the Loch Skerrols Thrust. The flattening strain ellipsoid in the thrust zone may be explained as due to a superposition of simple shear during thrusting over an initial flattening strain associated with buckle shortening of the Jura Quartzite. This implies that the Loch Skerrols Thrust is a break thrust.

Acknowledgements—Much of this work was done during the tenure of a state scholarship at Imperial College, London. The author is grateful to the late Janet Watson for her constant encouragement. Constructive criticisms by two anonymous reviewers and David J. Sanderson greatly helped in improving an earlier version. Facilities at the Indian Statistical Institute helped towards completion of this contribution.

REFERENCES

Amos, B. J. 1959. Geology of the Bowmore district. Unpublished Ph.D. thesis. University of London.

Anderton, R. 1988. Dalradian slides and basin development: a radical interpretation of stratigraphy and structure in the SW and Central Highlands of Scotland. *J. geol. Soc. Lond.* **145**, 669–678.

Bailey, E. B. 1917. The Islay Anticline. *Q. Jl geol. Soc. Lond.* **69**, 280–305.

Berthé, D., Choukroune, P. & Jegouzo, P. 1979. Orthogneiss, mylonite and non-coaxial deformation of granites: the example of the South Armorican Shear Zone. *J. Struct. Geol.* **1**, 31–42.

Borradaile, G. J. 1979. Strain study of the Caledonides in the Islay region, SW Scotland: implications for strain histories and deformation mechanisms in greenschist. *J. geol. Soc. Lond.* **136**, 77–88.

Bouchez, J.-L. 1977. Plastic deformation of quartzites at low temperature in an area of natural strain gradient. *Tectonophysics* **39**, 25–50.

Bouchez, J.-L., Lister, G. S. & Nicolas, A. 1983. Fabric asymmetry and shear sense in movement zones. *Geol. Rdsch.* **72**, 401–419.

Bouchez, J.-L. & Pêcher, A. 1976. Microstructures and quartz preferred orientations in quartzites of the Annapurna area (central Nepal) in the proximity of the Main Central thrust. *Himalayan Geology* **6**, 118–132.

Brunel, M. 1980. Quartz fabrics in shear zone mylonites: evidence for a major imprint due to late strain increments. *Tectonophysics* **64**, T33–T44.
Burg, J.-P. & Laurent, Ph. 1978. Strain analysis of a shear zone in a granodiorite. *Tectonophysics* **47**, 15–42.
Carreras, J., Estrada, A. & White, S. H. 1977. The effect of folding on the *c*-axis fabric of a quartz-mylonite. *Tectonophysics* **39**, 3–24.
Christie, J. M. 1963. The Moine Thrust in the Assynt region, NW Scotland. *Univ. Calif. Publs geol. sci.* **40**, 345–419.
Christie, J. M. & Ord, A. 1980. Flow stress from microstructures of mylonites: examples and current assessment. *J. geophys. Res.* **85**, 6253–6262.
Christie, J. M., Ord, A. & Koch, P. S. 1980. Relationship between recrystallized grain size and flow stress in experimentally deformed quartzite. *Eos* **61**, 377.
Dunnet, D. 1969. A technique of finite strain analysis using elliptical particles. *Tectonophysics* **7**, 117–136.
Etheridge, M. A. & Wilkie, J. C. 1979. The geometry and structure of QP mylonite zones—a field test of the recrystallized grain-size palaeopiezometer, analysis of actual fault zones in bedrock. *U.S. Geol. Survey* Open file Rep. **179–1239**, 448–504.
Fairbairn, H. W. 1949. *Structural Petrology of Deformed Rocks*. Addison-Wesley, Reading, Massachusetts.
Fairchild, I. J. 1980. The structure of NE Islay. *Scott. J. Geol.* **16**, 189–197.
Fitches, W. R. & Maltman, A. J. 1984. Tectonic development and stratigraphy at the western margin of the Caledonides: Islay and Colonsay, Scotland. *Trans. R. Soc. Edinb. Earth Sci.* **75**, 365–382.
Garson, M. S. & Plant, J. 1972. Possible dextral movements on the Great Glen and Minch faults in Scotland. *Nature* **240**, 31–35.
Hobbs, B. E., Means, W. D. & Williams, P. F. 1976. *An Outline of Structural Geology*. John Wiley & Sons, New York.
House, W. M. & Gray, D. R. 1982. Displacement transfer at thrust terminations in Southern Appalachians—Saltville Thrust as example. *Bull. Am. Ass. Petrol. Geol.* **66**, 830–842.
Kennedy, W. Q. 1946. The Great Glen Fault. *Q. Jl geol. Soc. Lond.* **102**, 41–76.
Kohlstedt, D. L. & Weathers, M. S. 1980. Deformation induced microstructures, palaeopiezometers and differential stresses in deeply eroded fault zones. *J. geophys. Res.* **85**, 6269–6285.
Lister, G. S. & Hobbs, B. E. 1980. The simulation of fabric development during plastic deformation and its application to quartzite: the influence of deformation history. *J. Struct. Geol.* **2**, 355–370.
Lister, G. S. & Price, G. P. 1978. Fabric development in a quartz–feldspar mylonite. *Tectonophysics* **49**, 37–78.
Lister, G. S. & Williams, P. F. 1979. Fabric development in shear zones: theoretical controls and observed phenomena. *J. Struct. Geol.* **1**, 283–297.
Malvern, L. E. 1969. *Introduction to the Mechanics of a Continuous Medium*. Prentice-Hall, Englewood Cliffs, New Jersey.
Mercier, J. C., Anderson, D. A. & Carter, N. L. 1977. Stress in the lithosphere, inferences from steady state flow in rocks. *Pure & Appl. Geophys.* **115**, 199–226.
Nicolas, A. & Poirier, J. P. 1976. *Crystalline Plasticity and Solid State Flow in Metamorphic Rocks*. John Wiley & Sons, London.
Ord, A. & Christie, J. M. 1984. Flow stresses from microstructures in mylonitic quartzites from the Moine Thrust Zone, Assynt area, Scotland. *J. Struct. Geol.* **6**, 639–654.
Passchier, C. W. 1983. The reliability of asymmetric *c*-axis fabrics of quartz to determine sense of vorticity. *Tectonophysics* **99**, T9–T18.
Ramsay, J. G. 1967. *Folding and Fracturing of Rocks*. McGraw-Hill, New York.
Ramsay, J. G. & Graham, R. H. 1970. Strain variation in shear belts. *Can. J. Earth Sci.* **7**, 786–813.
Robin, P. Y. F. 1977. Determination of geologic strain using randomly oriented strain markers of any shape. *Tectonophysics* **42**, T7–T16.
Saha, D. 1984. Deformation phases and minor intrusions from SW Argyllshire: implications with respect to Caledonian tectonics. Unpublished Ph.D. thesis, University of London.
Saha, D. 1985. A Fortran program for the determination of the magnitude and orientation of strain ellipsoid from two-dimensional strain ratios. *Q. Jl Geol. Miner. Metall. Soc. India* **57**, 139–158.
Sanderson, D. J. 1976. The superposition of compaction and plane strain. *Tectonophysics* **30**, 35–54.
Simpson, C. 1980. Oblique girdle orientation patterns of quartz *c*-axes from a shear zone in the basement core of the Maggia Nappe, Ticino, Switzerland. *J. Struct. Geol.* **2**, 243–246.
Simpson, C. & Schmid, S. M. 1983. An evaluation of criteria to determine the sense of movement in sheared rocks. *Bull. geol. Soc. Am.* **94**, 1281–1288.
Smith, C. S. & Guttman, L. 1953. Measurement of internal boundaries in 3-dimensional structures by random sectoring. *Trans. AIME* **197**, 81–87.
Tullis, J. 1977. Preferred orientation of quartz produced by slip during plane strain. *Tectonophysics* **39**, 87–102.
Tullis, J., Christie, J. M. & Griggs, D. T. 1973. Microstructures and preferred orientations of experimentally deformed quartzites. *Bull. geol. Soc. Am.* **84**, 297–314.
Tullis, J. & Yund, R. A. 1985. Dynamic recrystallization of feldspar. A mechanism for ductile shear zone deformation. *Geology* **13**, 238–241.
Turner, F. J. & Weiss, L. 1963. *Structural Analysis of Metamorphic Tectonics*. McGraw-Hill, New York.
Twiss, R. J. 1977. Theory and applicability of a recrystallized grain size palaeopiezometer. *Pure & Appl. Geophys.* **115**, 227–244.
Weathers, M. S., Bird, J. M., Cooper, R. F. & Kohlstedt, D. L. 1979. Differential stresses determined from deformation induced microstructure of the Moine Thrust Zone. *J. geophys. Res.* **84**, 7459–7509.
White, S. H. 1976. The effects of strain on the microstructures, fabrics and deformation mechanism in quartzite. *Phil. Trans. R. Soc. Lond.* **283A**, 69–86.
White, S. H. 1979. Grain and subgrain size variation across a mylonite zone. *Contr. Miner. Petrol.* **870**, 193–202.
Wilkinson, S. B., Teall, J. J. H. & Peach, B. N. 1907. The geology of Islay. *Mem. geol. Surv. U.K.*
Willis, B. 1894. Mechanics of Appalachian structure. *U.S. geol. Surv. 13th Ann. Rept.* 213–281.
Wilson, C. J. L. 1975. Preferred orientation in quartz ribbon mylonites. *Bull. geol. Soc. Am.* **86**, 968–974.

APPENDIX

Reference axes of a rectangular Cartesian co-ordinate frame are chosen as follows:

x—parallel to shear direction or 'direction of tectonic transport';
z—normal to the shear-zone boundary or thrust plane; thus xy is the thrust plane.

The λ_2 axis of an *initial* (pre-thrusting stage in the text) triaxial strain ellipsoid coincides with the y axis; x axis makes an angle θ with λ_1 axis. θ is positive measured in an anticlockwise direction from x axis. γ is the amount of shear strain (a left-handed, anti-clockwise shear reckoned positive). The deformation is equivoluminal.

Referred to the principal strain axes, the deformation gradient tensor for an *initial* triaxial strain is reduced to the diagonal form

$$\begin{bmatrix} \lambda_1^{1/2} & 0 & 0 \\ 0 & \lambda_2^{1/2} & 0 \\ 0 & 0 & \lambda_3^{1/2} \end{bmatrix}.$$

For the above choice of reference co-ordinate frame, the reference axes and the principal strain axes are related by the direction cosine matrix

$$\begin{bmatrix} \cos\theta & 0 & \sin\theta \\ 0 & 1 & 0 \\ -\sin\theta & 0 & \cos\theta \end{bmatrix}.$$

The effect of the superposition of simple shear is obtained through pre-multiplication by a simple shear deformation of the initial deformation matrix. The total deformation matrix, $\mathbf{D}$ is thus given by

$$\mathbf{D} = \underbrace{\begin{bmatrix} 1 & 0 & -\gamma \\ 0 & 1 & 0 \\ 0 & 0 & 1 \end{bmatrix}}_{\text{simple shear}} \times \underbrace{\begin{bmatrix} \cos\theta & 0 & \sin\theta \\ 0 & 1 & 0 \\ -\sin\theta & 0 & \cos\theta \end{bmatrix}}_{\text{direction cosines}} \times \underbrace{\begin{bmatrix} \lambda_1^{1/2} & 0 & 0 \\ 0 & \lambda_2^{1/2} & 0 \\ 0 & 0 & \lambda_3^{1/2} \end{bmatrix}}_{\text{triaxial strain}}$$

$$= \begin{bmatrix} \lambda_1^{1/2}(\cos\theta + \gamma \sin\theta) & 0 & \lambda_3^{1/2}(\sin\theta - \gamma\cos\theta) \\ 0 & \lambda_2^{1/2} & 0 \\ -\lambda_1^{1/2}\sin\theta & 0 & \lambda_3^{1/2}\cos\theta \end{bmatrix} \cdot \quad \text{(A.1)}$$

Then,

$$\mathbf{DD}^{\mathrm{T}} = \begin{bmatrix} \lambda_1(\cos\theta + \gamma\sin\theta)^2 + \lambda_3(\sin\theta - \gamma\cos\theta)^2 & 0 & \lambda_3\cos\theta(\sin\theta - \gamma\cos\theta) - \lambda_1\sin\theta(\cos\theta + \gamma\sin\theta) \\ 0 & \lambda_2 & 0 \\ \lambda_3\cos\theta(\sin\theta - \gamma\cos\theta) - \lambda_1\sin\theta(\cos\theta + \gamma\sin\theta) & 0 & \lambda_1\sin^2\theta + \lambda_3\cos^2\theta \end{bmatrix}. \quad \text{(A.2)}$$

$\mathbf{DD}^{\mathrm{T}}$ is the inverse of the Cauchy deformation tensor (Malvern 1969). This is a symmetrical tensor which has eigenvalues equal to the principal quadratic elongation ($\overline{\lambda}_i$, $i = 1, 3$) and eigenvectors parallel to the principal axes.

Once the elements of $\mathbf{DD}^{\mathrm{T}}$ matrix are calculated for a set of $\lambda_1, \lambda_2, \lambda_3$, θ and γ values, the eigenvalues are calculated using NAG routines on an EC 1033 mainframe computer of the Indian Statistical Institute. The resulting strain ellipsoid shapes are shown on Flinn plots only for two limiting values and one intermediate value of the obliquity, $\theta = 0°$, 90° and 50°, respectively (Figs. 7a–c in the main body of the text). Calculations were also done for other obliquities, $0° \leqq \theta \leqq 90°$ at 10° increments. These results are in conformity with the general observation made earlier and available on request.